Received: 22 February 2018 | Revised: 22 June 2018 | Accepted: 25 July 2018

DOI: 10.1002/mrm.27496

FULL PAPER

Magnetic Resonance in Medicine

Reduction of lipid contamination in MR spectroscopy imaging using signal space projection

Shang-Yueh Tsai[1,2] | **Yi-Ru Lin**[3] | **Hsin-Yu Lin**[3] | **Fa-Hsuan Lin**[4]

[1]Graduate Institute of Applied Physics, National Chengchi University, Taipei, Taiwan

[2]Research Center for Mind, Brain and Learning, National Chengchi University, Taipei, Taiwan

[3]Department of Electronic and Computer Engineering, National Taiwan University of Science and Technology, Taipei, Taiwan

[4]Institute of Biomedical Engineering, National Taiwan University, Taipei, Taiwan

Correspondence
Shang-Yueh Tsai, NO. 64, Sec. 2, ZhiNan Road, Wenshan District, Taipei City 11605, Taiwan.
Email: sytsai@nccu.edu.tw

Funding information
This work was supported in part by grants from the Ministry of Science and Technology, Taiwan (MOST 106-2221-E-004-001, 105-2221-E-004-003, 105-2420-H-004-003-MY2).

Purpose: Lipid contamination can complicate the metabolite quantification in MR spectroscopic imaging (MRSI). In addition to various experimental methods demonstrated to be feasible for lipid suppression, the postprocessing method is beneficial in the flexibility of applications. In this study, the signal space projection (SSP) algorithm is proposed to suppress the lipid signal in the MRSI.

Methods: The performance of lipid suppression using SSP and SSP combined with the Papoulis-Gerchberg (PG) algorithm (PG+SSP) is examined in 2D MRSI data and the results were compared with outer volume saturation (OVS) methods. Up to 10 lipid spatial components were extracted by SSP from lipid signals in the range of 0.8~1.5 ppm.

Results: Our results show that most lipid signals were found in the first 4 to 5 components and that lipid signals on the spectra can be suppressed using 4 to 5 components. Metabolites concentrations were quantified using LCModel. Two regions of interest (ROIs) were manually selected on the peripheral and inner brain regions. The quantification of metabolites in terms of fitting reliability (CRLB) and spatial variations within ROIs (SpaVar) is improved using SSP. When 5 to 6 components were used in SSP and PG+SSP, the metabolite concentrations and the associated SpaVar and CRLB are at the same level as those from the OVS.

Conclusion: We have demonstrated that the SSP method can be used to suppress the lipid signals of MRSI and SSP with 5 to 6 components is suggested to have a similar suppression performance as the OVS method.

KEYWORDS

lipid suppression, MR spectroscopic imaging, out volume saturation, Signal space projection

1 | INTRODUCTION

Lipid contamination originating from the Gibbs ringing artifacts may complicate the metabolite quantification in MR spectroscopic imaging (MRSI) at short echo time. Intense subcutaneous lipid signal extended from the original location to the inner brain area through the ringing may cause abrupt signal change, which results in serious distortion in the spectral baseline. Previously, several experimental methods have been proposed to suppress the lipid signal by RF-pulses applied during or before the data acquisition. One commonly used method implemented in the clinical system is outer

volume saturation (OVS) bands applied at the perimeter of the brain[1–4] to suppress the lipid signals based on geometric locations of the lipids.

The suppression scheme was further improved by considering field inhomogeneity using the BISTRO algorithm[5] and by considering T1 and B1 effects using the SELOVS algorithm,[6] which has been shown to be useful in a high-field system.[7,8] Typically, 6 to 10 OVS bands manually positioned around the brain can efficiently suppress subcutaneous lipids in a 2D MRSI plane. However, for 3D MRSI, the precise lipid suppression along the brain shape while maintaining the metabolite signal in the cortical region needs a great number of OVS bands. The placement of OVS bands surrounding the 3D imaging volume is a complicated and time-consuming procedures for operators. Although automated positioning of 12 to 16 OVS bands in 3D MRSI have been proposed,[9,10] the number of OVS bands is still limited in consideration of the specific absorption rate (SAR) and suppression efficiency.[11]

Another lipid suppression strategy is the lipid nulling with inversion recovery pulses.[12,13] This method is based on the differences in spin-lattice relaxation rates between the metabolite and lipid signals. A broadband inversion recovery pulse is applied and data acquisition starts at a delay of inversion time that corresponds to the null point of lipid T1 relaxation. It has been shown that the lipid signal can be effectively suppressed using single or dual inversion recovery schemes.[13] Although the suppression of lipid signals is accompanied by loss of metabolite signal, the metabolite concentrations can be corrected based on prior knowledge about the T1 of metabolites. Under some loss of the SNR, this method has been shown to be practical in 3D MRSI[14–16] and has been applied in clinical studies.[17,18] To suppress the lipid signal without affecting metabolite signals, frequency selective pulses applied either alone or in combination with water suppression pulses can be considered.

The dual-band suppression schemes are developed using dual-band RF pulse integrated with OVS bands, which create a pass band between 4.2 ppm and 1.8 ppm on the spectrum to suppress both lipid and water resonances.[19] This method has been integrated into the spectral editing method for measuring GABA images in 2D and 3D MRSI.[20,21] However, the suppression efficiency of frequency selective suppression is relatively sensitive to field homogeneity. The metabolite signal may be partially saturated at brain regions with field inhomogeneity. These experimental methods have been implemented in a clinical system and have been shown to be useful in 2D and 3D MRSI. However, the complete removal of lipid signals without significant interference with neighboring signals from brain metabolites is still challenging due to the tradeoff of these experimental methods. Additionally, the use of extra RF-pulses may raise the SAR, which may lower the flexibility of these methods particularly at high fields.

TABLE 1 Metabolite concentrations, CRLB, and the number of voxels of NAA and tCr of the MRS phantom with lipid (w. lip), without lipid (wo, lip), and lipid suppression using SSP1~10a[b]

No. of voxels (%)	w. lip	SSP1	SSP2	SSP3	SSP4	SSP5	SSP6	SSP7	SSP8	SSP9	SSP10	wo. lip
NAA	82.28	83.54	86.71	87.34	89.24	92.41	95.57	93.04	92.41	92.41	89.87	100
tCr	73.42	72.78	75.32	75.32	77.22	88.38	93.54	94.81	91.01	94.18	90.38	100
Conc. (mM)	w. lip	SSP1	SSP2	SSP3	SSP4	SSP5	SSP6	SSP7	SSP8	SSP9	SSP10	wo. lip
NAA	29.7 ± 14.7	25.7 ± 4.9	25.4 ± 4.8	27.2 ± 4.5	23.1 ± 4.3	29.6 ± 3.2	25.1 ± 4.0	22.3 ± 3.6	22.7 ± 3.8	22.2 ± 3.8	21.7 ± 3.2	18.7 ± 0.7
tCr	11.1 ± 1.8	10.8 ± 1.3	10.6 ± 1.1	10.5 ± 1.0	10.6 ± 1.3	10.7 ± 1.5	10.5 ± 1.4	10.3 ± 1.2	10.5 ± 1.3	10.5 ± 1.3	10.4 ± 1.1	10.3 ± 0.7
CRLB (%)	w. lip	SSP1	SSP2	SSP3	SSP4	SSP5	SSP6	SSP7	SSP8	SSP9	SSP10	wo. lip
NAA	9.2 ± 6.4	8.6 ± 5.3	8.2 ± 4.9	8.2 ± 5.2	8.3 ± 5.3	8.3 ± 5.1	8.2 ± 5.0	7.9 ± 4.9	8.0 ± 5.7	7.6 ± 4.8	7.6 ± 4.8	3.0 ± 0.5
tCr	12.1 ± 6.6	11.2 ± 5.6	11.3 ± 6.0	10.8 ± 5.3	10.6 ± 5.3	10.5 ± 5.2	10.6 ± 5.3	10.7 ± 5.3	9.8 ± 4.7	10.5 ± 5.2	10.0 ± 5.0	4.0 ± 0.6

[a]Abbreviation: CRLB, ; MRS, MR spectroscopy; Cr, creatine.
[b]The values are shown by mean ± SD over the ROI manually selected to cover the inner region of the MRS phantom.

Alternatively, the lipid contamination can also be reduced using a data reconstruction strategy. Because Gibb's ringing artifacts are the side lobe of the point spread function after the Fourier transform on the limited sample point in the spatial dimension (k-space), improvement can be achieved by acquiring an additional k-space sample over a spherical k-space volume and varying the number of averages acquired in proportion to the desired spatial filter.[22–24] However, the requirement of additional samples prolongs the acquisition time. As a lengthy scan time is already a major concern for the MRSI applications, this procedure significantly decreases the practicability of these methods. Therefore, some rapid acquisition methods with a modified k-space trajectory have been proposed to reduce the data acquisition time for these sampling strategies.[25–27] As the lipid suppression of experimental and data reconstruction methods are based on the modification of data acquisition strategies, the implementation of these methods involves the modification of pulse sequence. The strategy choice for the lipid suppression is, therefore, limited, because it depends on the onsite technical support by the system provider.

On the other hand, lipid suppression by postprocessing methods offers extended flexibility; they can be directly applied on various applications of MRSI and can also be combined with reconstruction or experimental methods to improve the lipid suppression efficiency. One previous method based on the Papoulis-Gerchberg (PG) algorithm was proposed.[28] This method widens the k-space sampling of the lipid signal. Gibb's ringing artifacts can be reduced by extrapolating the lipid signal to the high k-space region. Otherwise, the lipid suppression can only rely on fitting the lipid signal with premodel lipid spectral lines.[29]

In this study, a postprocessing method based on the signal space projection (SSP) algorithm is proposed to suppress lipid signal in the MRSI. The SSP is a spatial filtering technique, which has been used for MEG and EEG analysis.[30,31] The concept of SSP is to extract spatial pattern of noise from the signal and remove them. Here, we take the metabolite as signal and the lipid as noise. The performance of lipid suppression of SSP alone and SSP integrated with the PG method is examined in in vivo 2D MRSI data without lipid suppression and is compared with the performance of lipid suppression using OVS.

2 | METHODS

2.1 | Lipid suppression by PG and SSP algorithms

For the PG algorithm, the original 32 × 32 MRSI data were first resized to 128 × 128 using zero-filling in k-space and were then transformed into spatial-spectral domain. The lipid image, L(x,y), was calculated from the resized spatial-spectral MRSI data by integration of the signal in the lipid range (0.8~1.5 ppm). The lipid mask, M(x,y), was automatically

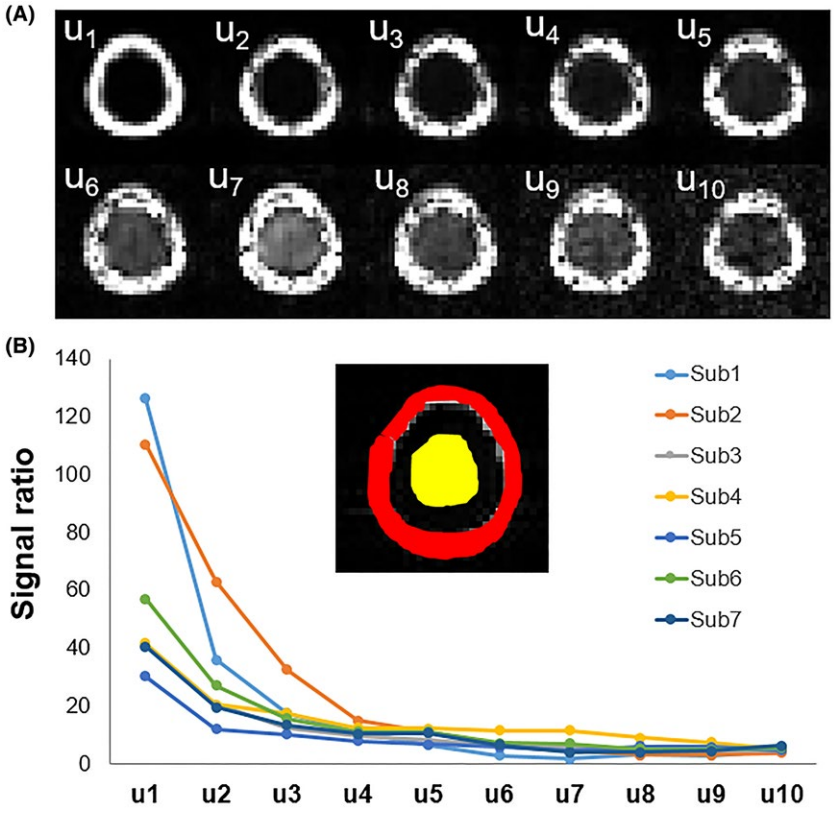

FIGURE 1 A, One to 10 spatial components of lipids from a subject and (B) the ratio of signal between the lipid and brain regions for 10 spatial components of lipids from 7 subjects. A lipid projection image from the sum of the magnitude signals in the range of 0.3 ppm to 1.8 ppm from a subject was shown in (B) overlay with manually selected ROIs of the subcranial lipid (red) and the inner brain regions (yellow). The lipid region is defined to cover the subcranial lipid signal and the brain region is defined inside the brain. Note that most lipid signals are extracted in the first 5 components and the signal ratio drops to a consistent level from the 4th component

defined on the L(x,y) using an initial threshold ϵ. Then, lipid signals were extracted by applying M(x,y) on the resized spatial-spectral MRSI data. The lipid signals were transformed to k-space and were used to update the outer k-space of the original resized MRSI data while the inner 32 × 32 k-space was kept unchanged. This procedure completes one iteration. For each iteration, the threshold ϵ_n of $M_n(x, y)$ is updated based on the minimum value of $L_n(x,y)$, and a cost function is defined as the difference of mean square energy between n and n-1 iterations. The iteration continues until the mean square energy difference is less than 3×10^{-3} or the iteration reaches 100 times.[28]

For lipid suppression using the SSP algorithm, the MRSI data were Fourier transformed into spatial and spectral domain. The complex MRSI data were expressed as a 2D spatial-spectral matrix $\mathbf{D_{ori}}$ in the dimension of [$N_x \times N_y$, N_f], where N_x and N_y is the size of spatial matrixes, and N_f is the size of spectral points corresponding to 9.01 ppm to 0.32 ppm spectral range. A lipid matrix $\mathbf{D_{ori\text{-}lipid}}$ in the dimension of [$N_x \times N_y$, $N_{f\text{-}lipid}$] was generated from the lipid range (0.8~1.5 ppm) by extracting 42 spectral points (443 to 484) from the $\mathbf{D_{ori}}$. Singular value decomposition (SVD) of $\mathbf{D_{ori\text{-}lipid}}$ yields spatial-spectral characterizations of lipid signal as:

$$\mathbf{D_{ori-lipid}} = \mathbf{U_n} \times \mathbf{S_n} \times \mathbf{V_n^H} \tag{1}$$

$$\mathbf{U_n} = [\mathbf{u}_1, \ldots \mathbf{u_n}]$$

$$\mathbf{V_n} = [\mathbf{v}_1, \ldots \mathbf{v_n}]$$

$$\mathbf{S_n} = diag([s_1, \cdots s_n])$$

where $\mathbf{u_i}$ is the spatial component of the lipid, $\mathbf{v_i}$ is the spectral component of the lipid and s_i is the singular value. The lipid spatial pattern can then be extracted for lipid suppression by

$$\mathbf{P} = \mathbf{I} - \mathbf{U_m} \times \mathbf{U_m^H} \tag{2}$$

$$\mathbf{U_m} = [\mathbf{u}_1, \ldots \mathbf{u_m}]$$

$$\mathbf{D_{supp}} = \mathbf{P} \times \mathbf{D_{ori}} \tag{3}$$

where $\mathbf{U_m}$ represent the spatial pattern of the lipid signal of the first m components and the components are ordered from largest to smallest according to the singular values. $\mathbf{P}$ is the signal space projection matrix of the lipid suppression and $\mathbf{D_{supp}}$ is the spatial spectral matrix after lipid suppression.

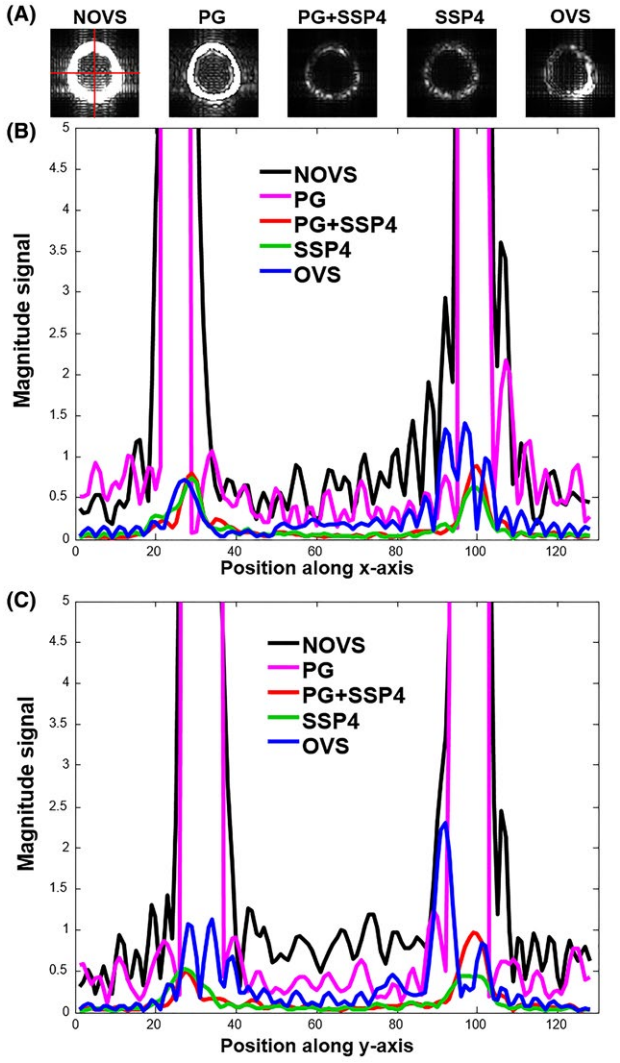

FIGURE 2 A, Spectral projection images (sum of magnitude signals) between 0.6 to 1.5 ppm from NOVS, PG, PG+SSP4, SSP4, and OVS. Central horizontal line (B) and central vertical line (C) of the projection images. Note that serious ringing artifacts can be found

2.2 | Experiments

MRSI experiments were performed on 7 healthy volunteers using a 3T scanner (Skyra, SIEMENS Medical Solutions, Erlangen, Germany) with a 32-channel head coil array. All volunteers submitted written informed consent in accordance with the Institutional Review Board approval. Before being included in this study, all participants gave their informed consent to undergo a protocol, which was approved by the Research Ethics Committee of National Chengchi University. T_1-weighted images, using a gradient echo sequence (TR/TE/flip angle, 250 ms/2.61 ms/70°; FOV, 256 × 256 mm^2; MAT, 128 × 128), were acquired for localizing the MRSI slice. MRSI data were acquired from a para-axial slice at the upper edge of ventricles using the following parameters: TR = 2 s, TE = 35 ms, flip angle = 90°, matrix size = 32 × 32,

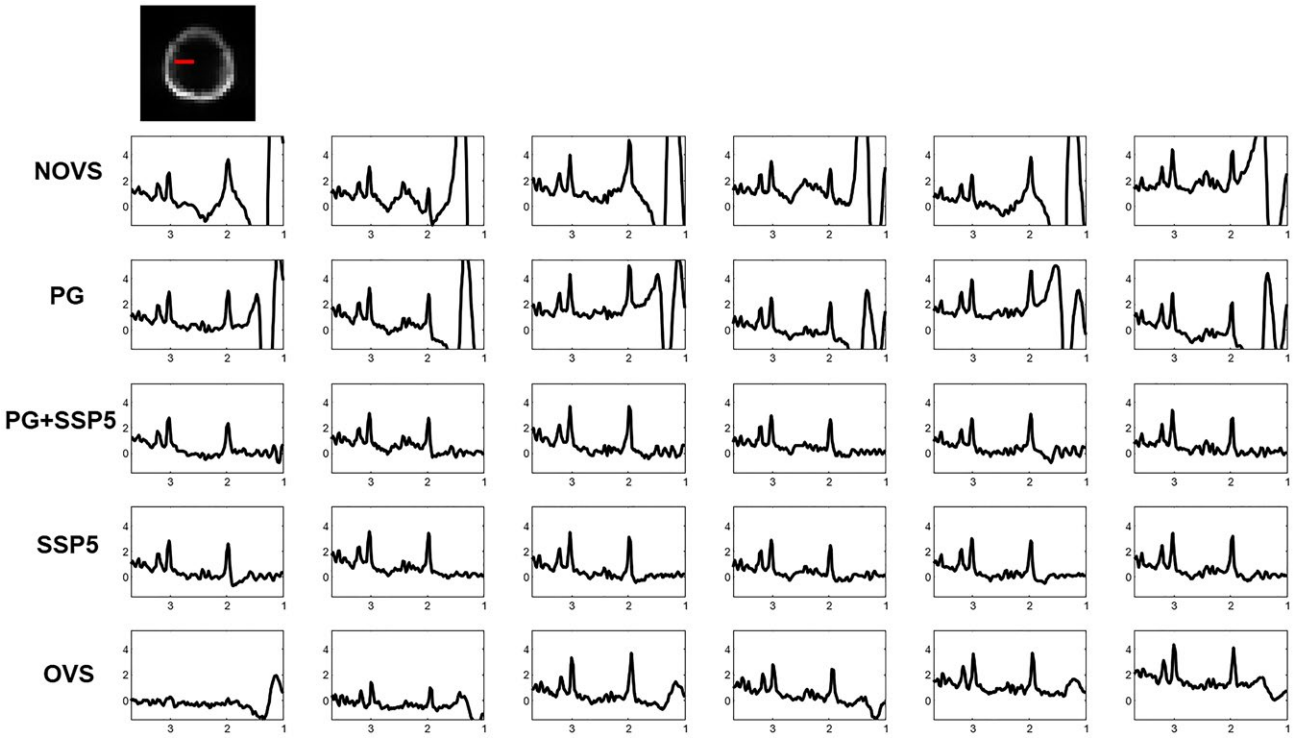

FIGURE 3 Spectra of NOVS, PG, PG+SSP5, SSP5, and OVS from a subject. The spectra are from voxels at the peripheral brain to the central brain as indicated in the image. The y index of voxels is 16 and the x index of voxels is 10-15 (left to right). Note that strong lipid artifacts can be found on NOVS even in the central brain. The spectra of SSP and PG+SSP are close to those of OVS, except the spectra at the peripheral brain (left), in which the metabolic signal is partly suppressed due to saturation bands

FOV = 220 × 220 mm^2, slice thickness = 15 mm, number of excitations = 4. The MRSI sequence includes a spin echo excitation and spatial-spectral echo planar acquisition, which has been described in previous reports.[3,4]

MRSI data sets were acquired with OVS and without OVS (NOVS). For the OVS scan, complete 8-slice outer volume suppression was applied along the perimeter of the brain to suppress lipid signal. A nonwater suppressed (NWS) reference scan was acquired using only one average as the reference for phase correction, calibration of metabolic signal. The total acquisition time for each subject is around 30 min including 11 min MRSI scans, 4 min T1 scan, and 10~15 min for adjustment, shimming, and spatial localization of MRSI scans.

To examine the performance of SSP methods, a MRS phantom with known concentrations of major metabolites was made using a container in the shape of cylinder (13 cm diameter and 12 cm height). The metabolites of the phantom include N-acetyl-L-aspartic acid (NAA, 20 mM), creatine hydrate (Cr, 10 mM), choline chloride (Cho, 3 mM), myo-inositol (mI, 7.5 mM), L-glutamic acid (Glu, 12 mM), sodium azide (0.1%), potassium phosphate monobasic (KH_2PO_4, 28 mM), potassium phosphate dibasic (K_2HPO_4, 72 mM). The MRS phantom was then put into another container in the shape of cylinder (16 cm diameter and 15 cm height) filled with oil (lard) as analogue of the subcranial lipids. The MRSI experiment was performed on the MRS phantom without lipid (wo. lip) and with lipid (w. lip) using the parameters: TR = 2 s, TE = 35 ms, flip angle = 90°, matrix size = 32 × 32, FOV = 192 × 192 mm^2, slice thickness = 20 mm. NWS scan was acquired.

2.3 | Postprocessing

For the MRSI data, standard postprocessing steps including temporal filtering, phase correction, and even-odd echo editing were performed.[32,33] The reconstructed spectral width after even/odd echo editing was 1086 Hz, with 512 complex-number data points. The phase correction was performed before averaging data from individual coils to reduce the possible artifacts caused by partial phase cancellation. Lipid suppression was applied on NOVS data using SSP combined with PG (PG+SSP), and using SSP alone. In this study, 10 components were extracted using SVD. According to the number of lipid components used for lipid suppression, data sets are named SSP1 to SSP10. For example, SSP1 means that only the first lipid component was used for lipid suppression, and SSP2 means that the 1st and 2nd lipid components were enrolled for lipid suppression.

The localized spectra were quantified by the LCModel software package (https://s-provencher.com/lcmodel.shtml).

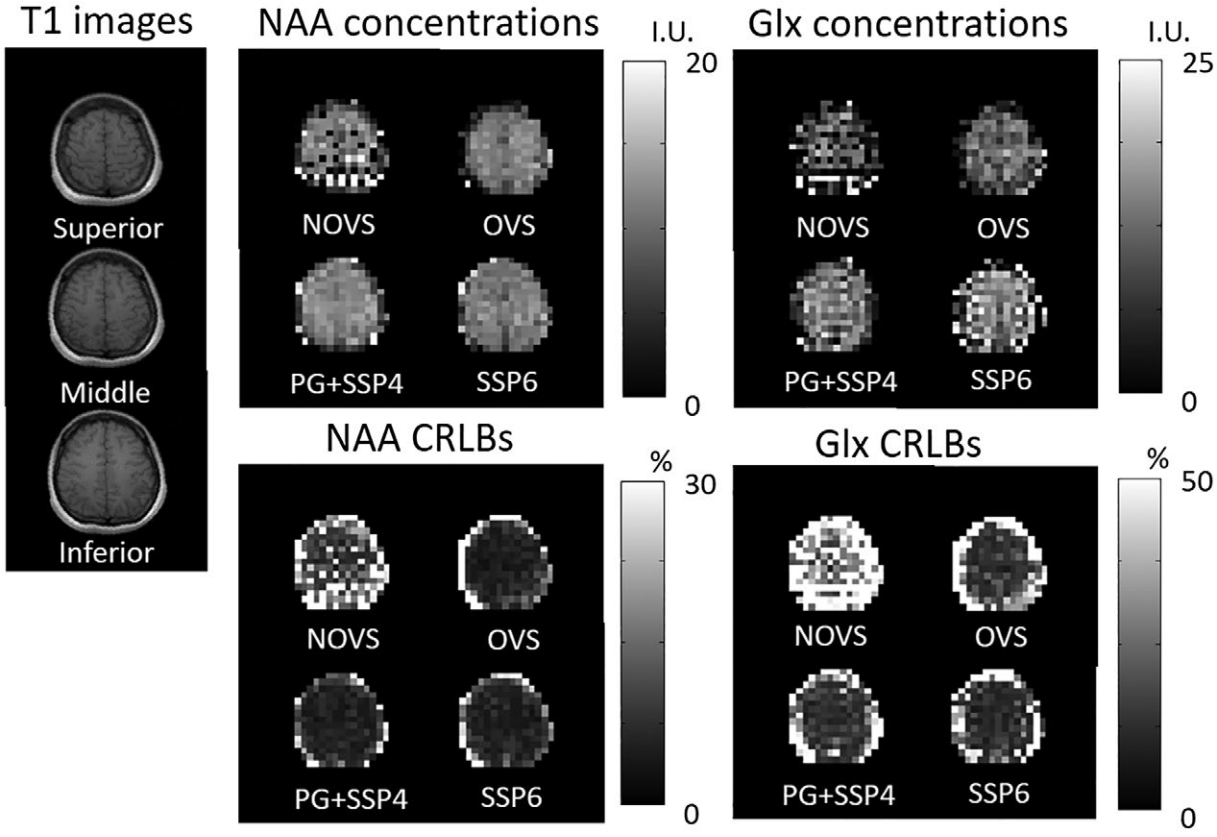

FIGURE 4 Metabolite concentration and CRLB maps of NAA and Glx from NOVS, OVS, SSP6, and PG+SSP4. The voxels are presented as black points when the LCModel is unable to quantify the metabolite on the spectra. Note that compared with those of NOVS, the concentration maps of OVS, PG+SSP4, and SSP6 are homogenous with less excluded voxels. The T1 images (3 mm) corresponding to superior, middle and inferior part of 15 mm MRSI slice are shown in the left

Basis sets for in vivo data included the following 18 metabolites: alanine (Ala), aspartate (Asp), creatine (Cr), gamma-amino-butyrate (GABA), glucose (Glc), glutamine (Gln), glutamate (Glu), glycerophosphocholine (GPC), phosphocholine (PCho), lactate (Lac), myo-inositol (mI), N-acetyl-aspartate (NAA), N-acetyl-aspartylglutamate (NAAG), scyllo-inositol (scyllo), and taurine (Tau). Basis sets for the phantom data included NAA, GPC, PCh, Cr, mI, and Glu. The macromolecules were excluded for the phantom data. Spectra were fitted between 0.5 and 4 ppm. Metabolic signals were calibrated to NWS data using the water scaling method. In this study, three metabolites in the brain were quantified in institutional units (I.U.): NAA=NAA+NAAG, tCr= Cr+PCr and Glx= Glu+Gln.

2.4 | Statistics

To examine the spatial lipid components extracted by SSP, two ROIs were manually selected on lipid projection image (0.3 ppm to 1.8 ppm) of each subject to cover the subcranial lipid region and the inner brain region. The ratio of signal in the lipid and brain regions was calculated for each spatial lipid component ($\mathbf{u}_1$ to $\mathbf{u}_{10}$) for each subject.

For the quantified metabolites by the LCModel, two ROIs were manually selected on each subject. One ROI was at the inner brain region and the other ROI was at the peripheral region of the brain close to the lipid region. The Cramer-Rao lower bounds (CRLB) were used as the error metric for the metabolite quantification. Expressed in concentration percentage, CRLB can be used as an indicator of the reliability for the quantification of metabolite concentrations. Voxels with CRLB > 30% for NAA and tCr and CRLB > 50% for Glx were excluded from the ROI analysis. The metabolite concentrations, CRLB, and number of voxel excluded by CRLBs within ROI were calculated for each subject using SSP and PG+SSP. To evaluate the spatial uniformity of quantified metabolite concentrations, the spatial variations of metabolite concentrations (SpaVar) within ROI were calculated as the standard deviation divided by the mean within ROI.

3 | RESULTS

The quantitative results of MRS phantom are summarized in Table 1. The number of voxels and the concentrations of NAA and tCr are at consistent level in 7th to 10th

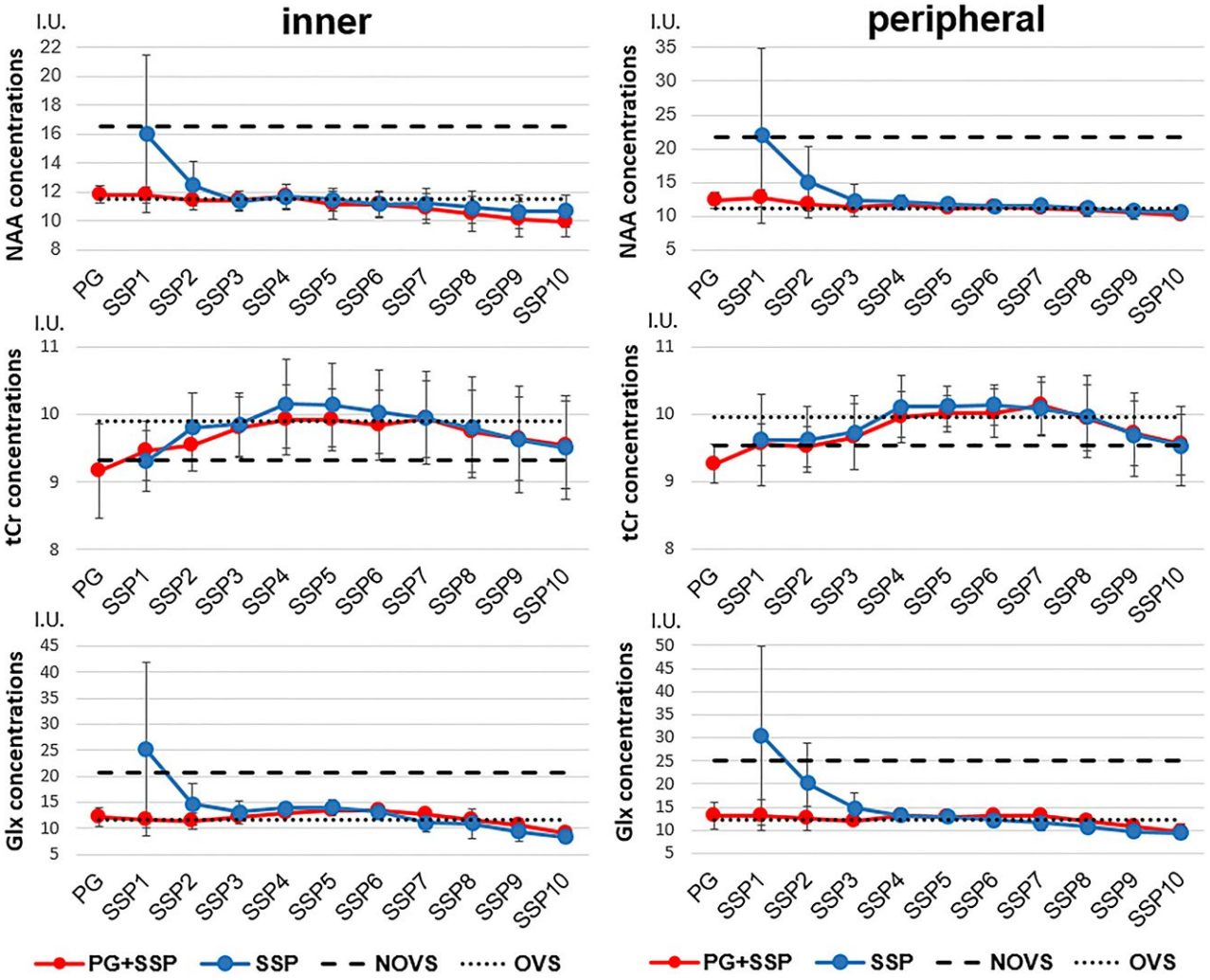

FIGURE 5 NAA, tCr, and Glx concentrations of the peripheral brain region and the inner brain region. The concentration level of NOVS and OVS are indicated as the dashed and dotted lines, respectively. The concentrations of SSP using 1 to 10 components and PG+SSP using components from 1 to 10 are shown with the error bars from the standard deviation between subjects. For NOVS, the concentrations and between-subject variation of NAA, tCr, and Glx are 16.6 ± 6.7 I.U., 9.3 ± 0.6 I.U., and 20.1 ± 11.1 I.U., respectively, for the inner brain and 21.7 ± 12.7 I.U., 9.5 ± 1.0 I.U., and 25.2 ± 16.3 I.U., respectively, for the peripheral brain. For OVS, the concentrations and between-subject variation of NAA, tCr, and Glx are 11.6 ± 0.6 I.U., 9.9 ± 0.6 I.U., and 11.6 ± 0.8 I.U., respectively, for the inner brain and 11.1 ± 0.7 I.U., 9.9 ± 0.5 I.U., 12.1 ± 0.5 I.U. for the peripheral brain. The results of SSP and PG+SSP using components more than 4 are at a consistent level as those of OVS

components. The concentrations of NAA (21.7 mM to 22.3 mM) and tCr (10.3 to 10.4 mM) are close to the concentrations of the phantom (NAA :20 mM, tCr: 10 mM). For NAA and tCr, the spatial variations of the concentrations and CRLB drop when more components are enrolled. However, the spatial variations and CRLB of SSP are higher than those from wo. lip, where the number of voxels are also less than those from wo. lip. The spectra of w. lip and wo. lip phantom are shown in Supporting Information Figure S1, which is available online. The spectra of w. lip phantom using SSP are shown Supporting Information Figure S2.

Figure 1 shows the intensities of the 10 spatial lipid components from the subject and the signal ratio of the lipid region to the brain region of 10 lipid spatial components from 7 subjects. The 10 spatial lipid components from the subject show that most lipid signals were extracted using the first 4 to 5 components (Figure 1A). Despite the variation of signal ratios across subjects (Figure 1B), the ratio drops to a consistent level (<20) after the 4th component. Figure 2 shows the projection (the sum of the magnitude signals) of the spectroscopic image in the lipid range (0.6~1.5 ppm) and the signal profiles of projection images from a subject. Clear ringing

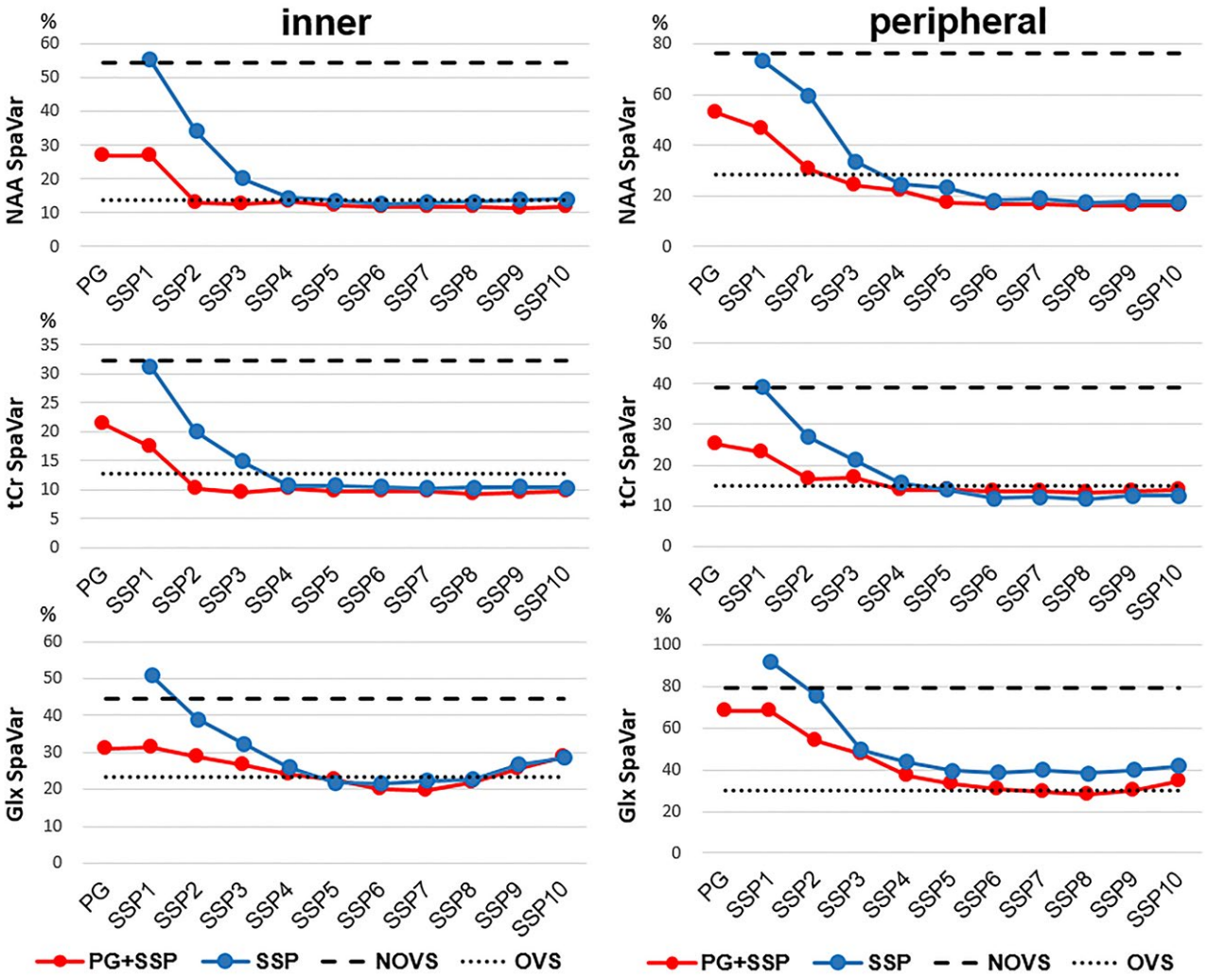

FIGURE 6 The spatial variation (SpaVar) over the peripheral brain region and the inner brain region of NAA, tCr, and Glx. The SpaVar of NOVS and OVS are indicated as dashed and dotted lines, respectively. The concentrations of SSP using 1 to 10 components and PG+SSP using components from 1 to 10 are shown with the error bars from the standard deviation between subjects. Note the SpaVar represents the homogeneity of quantified metabolites within the brain region. The SpaVar of NAA, tCr, and Glx are all larger in NOVS and decreased to a consistent level as those of OVS for SSP and PG+SSP using more than 4 components

pattern from the lipid contamination can be found on the projection images and signal profile of NOVS.

Lipid contamination is reduced by lipid suppression using OVS, but some residual lipid signals can still be found at the posterior region of the brain in this subject. Using PG, SSP and combined PG+SSP can also reduce the lipid contamination of NOVS data where the projection images and the signal profiles of SSP and SSP+PG are close to those from OVS. Figure 3 shows a series of representative spectra from the peripheral brain region to the central brain region. Strong lipid signals can be found on the spectra of NOVS even in the central brain. For PG, the lipid signal is lowered and three major metabolic peaks can be observed on the spectra. For SSP and PG+SSP, the lipid signal is further suppressed so that metabolic peaks can be clearly identified even at the peripheral brain region. The spectra of PG+SSP and SSP are similar to those from OVS but the metabolic peaks are not found on the spectra of OVS at the peripheral brain region.

Metabolite concentration maps of NAA and Glx and corresponding CRLB maps are shown in Figure 4. Voxels with unquantifiable metabolites can be found on the concentration maps of NOVS but are not found on OVS, SSP6, and PG+SSP4. The CRLBs of NOVS are also obviously higher than those of OVS, SSP6, and PG+SSP4. The concentrations and CRLBs of SSP6, PG+SSP4, and OVS show similar spatial distribution. The quantified concentrations of NAA, tCr, and Glx from the peripheral and the inner brain ROIs are shown in Figure 5. For NOVS, the concentrations and between-subject variations of NAA and Glx are higher than those of OVS. For both the inner and the peripheral brain regions, the concentrations and between-subject variations decreased to a consistent level for PG+SSP and SSP using

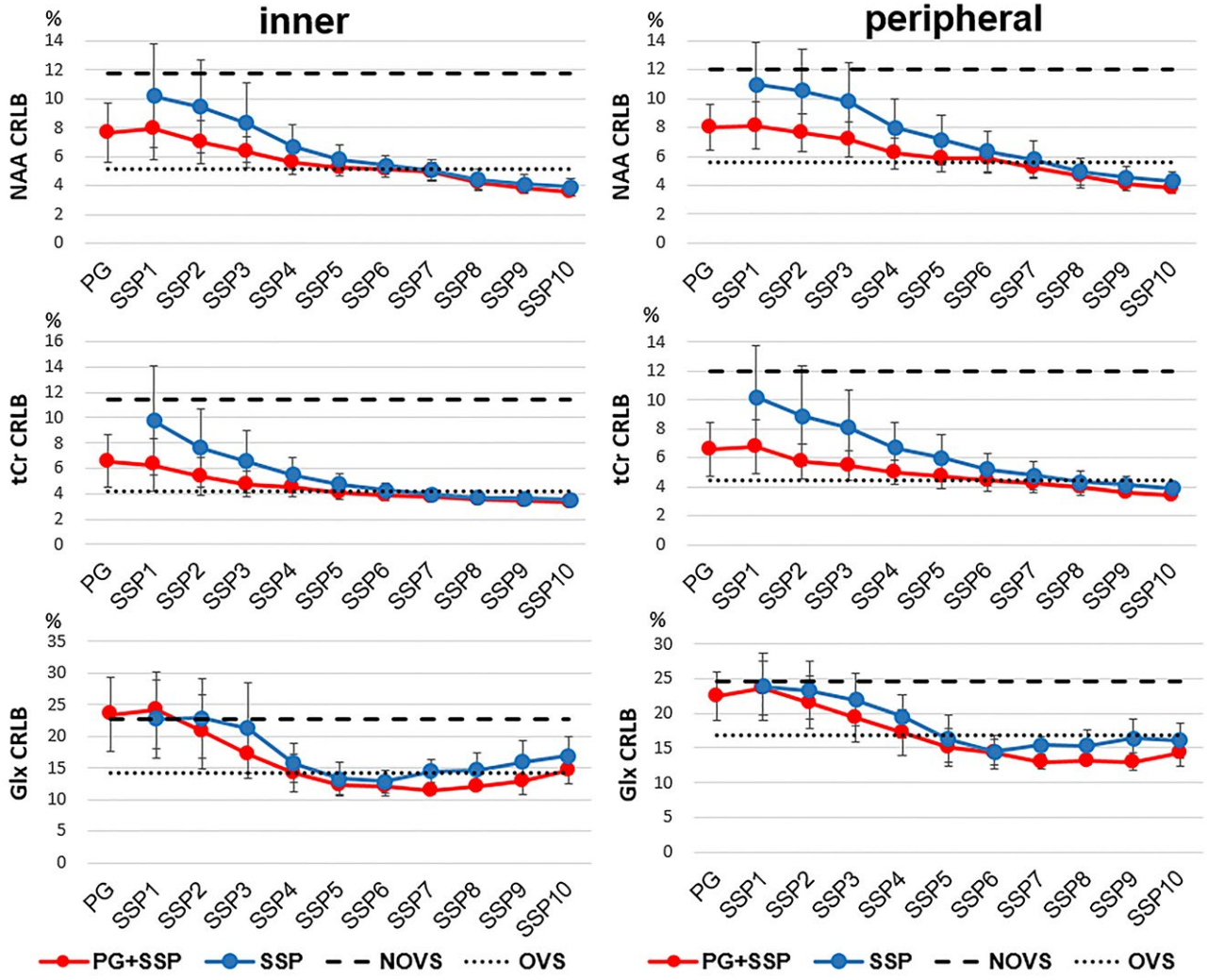

FIGURE 7 NAA, tCr, and Glx CRLB of the peripheral brain region and the inner brain region. The CRLB of NOVS and OVS are indicated as dashed and dotted lines, respectively. The CRLB of SSP using 1 to 10 components and PG+SSP using components from 1 to 10 are shown with the error bars from the standard deviation between subjects. For NOVS, the CRLB of NAA, tCr, and Glx are 11.7 ± 1.4%, 11.4 ± 1.6%, and 22.6 ± 3.5%, respectively, for the inner brain and 12.0 ± 1.0%, 12.0 ± 1.9%, and 24.6 ± 3.2%, respectively, for the peripheral brain. For OVS, the CRLB of NAA, tCr, and Glx are 5.1 ± 1.1%, 4.2 ± 1.2%, and 14.2 ± 2.7%, respectively, for the inner brain and 5.6 ± 0.9%, 4.4 ± 0.7%, and 16.8 ± 3.0%, respectively, for the peripheral brain. The CRLB of NAA and tCr decreased as more components were used. For Glx, the CRLBs decreased to 15% for SSP and PG+SSP using more than 5 components

more than 4 components and are close to the results of OVS. For tCr, higher between-subject variation (9.5 ± 1.0 I.U.) is found in the peripheral regions in NOVS. The SpaVar of metabolites are shown in Figure 6. The SpaVar of NOVS is much larger than those of OVS for NAA, tCr, and Glx in both the peripheral and the inner brain regions. The SpaVar of PG+SSP and SSP decreases to the level of OVS when more than 4 components were used for lipid suppression. The SpaVar in the peripheral region is larger than the SpaVar of the inner region. The CRLB are shown in Figure 7. For NOVS, the CRLBs of NAA and tCr are over 10% and the CRLBs of Glx are over 20%. The CRLBs of NAA and tCr decreased as more components were used in PG+SSP and SSP. The CRLBs of NAA and tCr can be lower than 8% when 5 components were used in SSP and PG+SSP. For Glx, the CRLBs of SSP and PG+SSP decreased to the level of OVS (<16%) when 5 components were used. The number of voxels that passed the CRLB criteria and were enrolled for the ROI analysis are shown in Figure 8. In NOVS, an average of 70~85% of voxels passed the 30% CRLB thresholds of NAA and tCr. For Glx, there were only 55~60% of voxels on average that were included in the ROI analysis. For OVS, an average of over 97% voxels passed the CRLB thresholds of NAA and tCr and approximately 90% voxels passed the thresholds of Glx. The number of voxels also increased to 97% for NAA and tCr and to 89% for Glx using PG+SSP and SSP with the

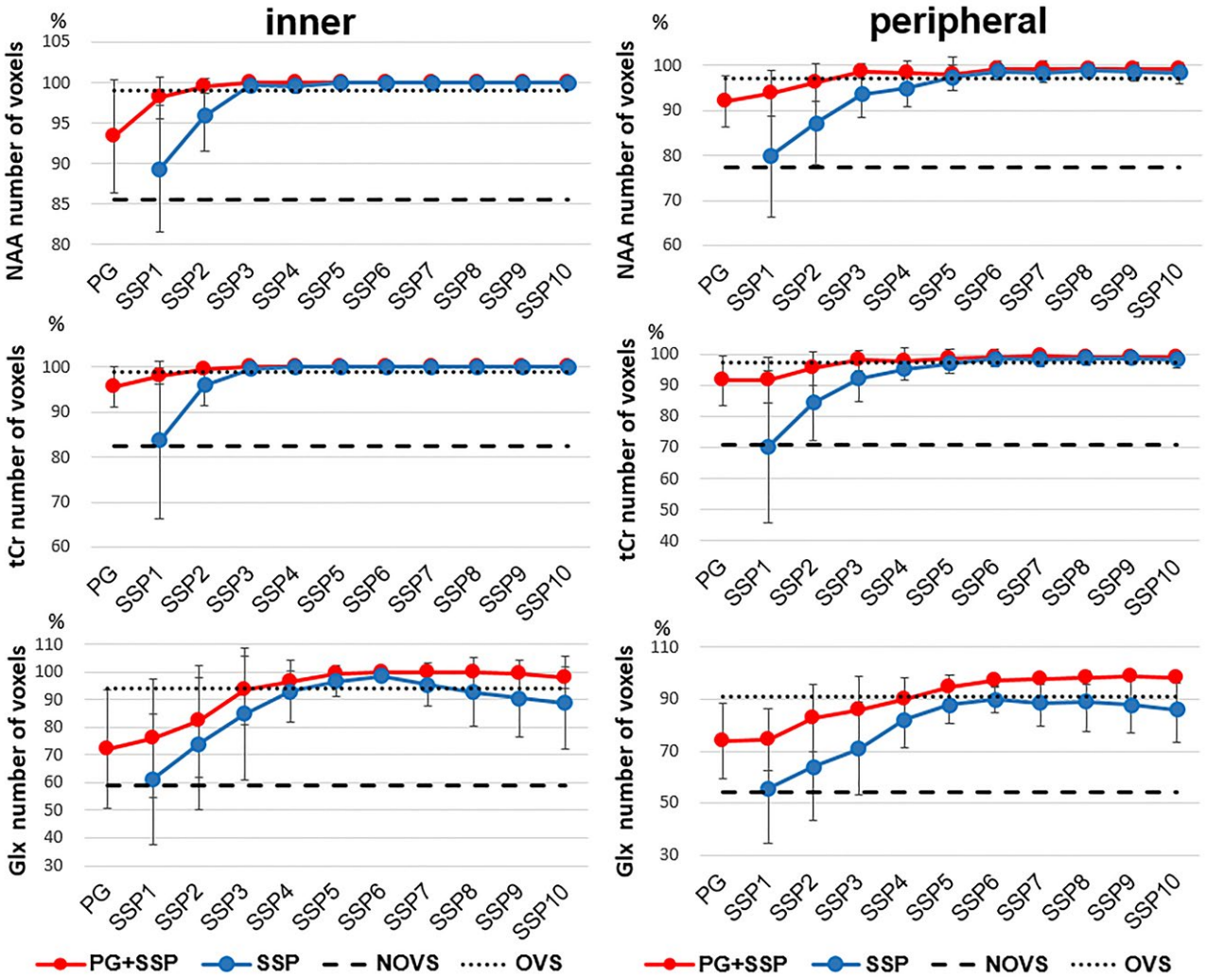

FIGURE 8 The number of voxels included in the ROI analysis for the peripheral brain region and the inner brain region. The percentage of NOVS and OVS are indicated as dashed and dotted lines, respectively. The number of voxels of SSP using 1 to 10 components and PG+SSP using components from 1 to 10 are shown with the error bars from the standard deviation between subjects. The rejection criteria of CRLB are over 30% for NAA and tCr and over 50% for Glx. More voxels pass the CRLB criterion using SSP and PG+SSP, and a consistent level is reached when 5 components were used

5 components that were used for lipid suppression. For both inner and peripheral brain regions, the lipid signals fitted by LCModel decreased when more components were used for PG+SSP and SSP. The results are shown in Supporting Information Figure S3.

4 | DISCUSSION

In this study, we have demonstrated that the proposed SSP algorithm can be used to suppress the lipid signals of MRSI data. Most lipid signals can be extracted in the first 5 components using SSP (Figure 1) and these lipid components can be used to suppress the lipid signal on the projection image (Figure 2) and the spectra (Figure 3). Lipid suppression by SSP can improve the quantification of metabolites in terms of fitting reliability (CRLB) and spatial variations (SpaVar). When 5 to 6 components of SSP were used, the quantified metabolite concentrations and the associated SpaVar, CRLBs are at the same level as those from the OVS (Figures 5–7). Therefore, we suggest using SSP or SSP+PG with 5 to 6 components for lipid suppression.

The quantified results (concentrations, SpaVar, CRLB, number of voxels) are at a consistent level when more than 4 lipid components were enrolled. As seen in the spectra using 4 components (Figure 3), the lipid signals on the spectra are significantly suppressed to have a flattened baseline similar to the spectra of OVS. There are some residual baseline fluctuations, possibly from the contributions of macromolecules. Compared with the metabolic peaks, these fluctuations are relatively small and they can usually be handled by the spectral fitting algorithm with presumed models. This observation

is in accordance with the results of the extracted lipid components (Figure 1), where most lipid signals are extracted at the first 5 components. When more components are used (>6), the baselines of the spectra can be further flattened. It is not clear if the baseline flattening more than what is shown in Figure 3 is beneficial for spectral fitting.

Furthermore, the original MRSI data ($\mathbf{D_{ori}}$) was projected onto the lipid spatial pattern ($\mathbf{U_m}$) composed of several lipid components ($\mathbf{u_1}$ to $\mathbf{u_{10}}$). When the lipid spatial pattern contains signal contributions from the inner brain, the metabolite signal can be partly suppressed. As shown in Figure 1, there are observable signal contributions from the inner brain on the components ($\mathbf{u_6}$ to $\mathbf{u_{10}}$). There is the possibility that metabolic signals are partly suppressed by the extracted spatial components when more components were enrolled, and this outcome may affect the quantification of metabolites on the spectra. Although this effect was not found in this study, 5 to 6 components are considered reasonable choices for the SSP for lipid suppression (Supporting Information Figure S4).

In this study, the OVS method was used as the comparison standard. We demonstrated that the SSP method can have similar lipid suppression performance to the OVS on 2D MRSI. Whether the SSP or PG+SSP method can have better lipid suppression than the OVS method is unknown. The major reason is that the OVS method has already been used as a routine protocol for the 2D MRSI. Up to 8 saturation bands are sufficient to cover the peripheral lipids surrounding the brain shape. Even if the OVS method cannot suppress all lipid signals, the residual lipids can usually be fitted using software constraints. However, OVS method may partially suppress the metabolic signal for voxels close to the saturation bands. This effect can be found on the spectra of OVS from the peripheral region (Figure 3). The SSP and SSP+PG methods have the potential to perform lipid suppression while retaining the metabolic signal at these regions (Figure 3). Another issue for OVS is the SAR, which limits the application of the OVS method on high-field system and 3D MRSI. The proposed SSP method can be integrated with the OVS methods to help lipid suppression under a limited number of OVS bands. The performance of lipid suppression using SSP and SSP integrated with OVS on the high field MRSI and 3D MRSI is under further investigation.

According to the results of MRS phantom, the performance of SSP using more components (7 to 10 components) reaches a consistent level in terms of mean concentrations and the spatial variations of the concentrations. This is in accordance with the findings from in vivo data. The mean concentrations are 10% difference from the known concentrations for NAA and 5% difference for tCr. The spatial variations still differ from those from wo. lip. This suggests that lipid contamination cannot be fully removed using the SSP method. We found that the lipid signals can be significantly reduced using SSP but there are some residual baseline distortions in the spectral range of 1.6~2.8 ppm (Supporting Information Figure S2). This could affect the baseline estimation on the quantification of NAA, and may be the reason for larger spatial variations in w. lip phantom using the SSP method.

There are several differences between the pattern of the lipid signals from w. lip phantom and from human brain. First, oil was filled in the outer container as analogue of lipids. Unlike the signals of the subracial regions in brain, which has mixed water and lipid signals, there are only lipid signals in the w. lip phantom (Supporting Information Figure S1). Other strategy should be considered in making the lipid layer for w. lip phantom such as bacon or mixed water and lipid solutions. Second, the lipid signals in w. lip phantom have narrower linewidth (Supporting Information Figure S1) compared with those from the healthy subjects (Figure 3). The lipid contaminations on the spectra show sharp signal fluctuations over the lipid range (Supporting Information Figure S2). For some voxels with sharp baseline fluctuations on the lipid range, LCModel have problems on the baseline estimation and failed to quantify the metabolite. This can be the reason why CRLB of NAA, tCr are higher in w. lip phantom than those in wo. lip phantom and there are 10% of voxels excluded in the ROIs (Table 1).

The postprocessing method has an advantage in the flexibility of applications. In this study, the SSP method is applied alone and combined with the PG method (SSP+PG). The results show that PG suppresses the lipid signal to a certain level and SSP can further suppress the lipid signals. Using SSP alone can have the same suppression performance as PG+SSP but with more components (Figures 6, 7). This does not mean that SSP can replace PG, but indicates that SSP can be integrated with other post processing strategies. As each algorithm may have its limitations, suppression efficiency may be altered under various situations. It is beneficial to combine various methods. Because the lipid components are extracted using MRSI data in the lipid range, there is the possible problem raised by the field inhomogeneity in the definition of the lipid region. Additionally, there are various experimental methods proposed for lipid suppression. SSP not only can be considered as an alternative but can also be integrated with these experimental methods.

In conclusion, a postprocessing method using SSP is demonstrated to be feasible for lipid suppression. For a 2D MRSI, the performance of lipid suppression is close to the OVS method in terms of the CRLB and the SpaVar using SSP with 5~6 components.

ACKNOWLEDGMENTS

The authors thank the Taiwan Mind & Brain Imaging Center (TMBIC) and National Chengchi University for the instrument availability. The TMBIC is supported by the Ministry of Science and Technology, Taiwan.

ORCID

Shang-Yueh Tsai http://orcid.org/0000-0002-6310-4750

REFERENCES

1. Shungu DC, Glickson JD. Sensitivity and localization enhancement in multinuclear in vivo NMR spectroscopy by outer volume presaturation. *Magn Reson Med* 1993;30:661–671.
2. Duyn JH, Gillen J, Sobering G, van Zijl PC, Moonen CT. Multisection proton MR spectroscopic imaging of the brain. *Radiology*. 1993;188:277–282.
3. Tsai SY, Wang WC, Lin YR. Comparison of sagittal and transverse echo planar spectroscopic imaging on the quantification of brain metabolites. *Journal of neuroimaging* 2015;25:167–174.
4. Tsai SY, Lin YR, Wang WC, Niddam DM. Short- and long-term quantitation reproducibility of brain metabolites in the medial wall using proton echo planar spectroscopic imaging. *NeuroImage*. 2012;63:1020–1029.
5. Luo Y, de Graaf RA, DelaBarre L, Tannus A, Garwood M. BISTRO: an outer-volume suppression method that tolerates RF field inhomogeneity. *Magn Reson Med*. 2001;45:1095–1102.
6. Henning A, Schar M, Schulte RF, Wilm B, Pruessmann KP, Boesiger P. SELOVS: brain MRSI localization based on highly selective T1- and B1- insensitive outer-volume suppression at 3T. *Magn Reson Med*. 2008;59:40–51.
7. Bogner W, Gruber S, Trattnig S, Chmelik M. High-resolution mapping of human brain metabolites by free induction decay (1) H MRSI at 7 T. *NMR Biomed*. 2012;25:873–882.
8. Henning A, Fuchs A, Murdoch JB, Boesiger P. Slice-selectiveFID acquisition, localized by outer volume suppression (FIDLOVS) for (1)H-MRSI of the human brain at 7 T with minimal signal loss. *NMR Biomed*. 2009;22:683–696.
9. Yung KT, Zheng W, Zhao C, Martinez-Ramon M, van der Kouwe A, Posse S. Atlas-based automated positioning of outer volume suppression slices in short-echo time 3D MR spectroscopic imaging of the human brain. *Magn Reson Med*. 2011;66:911–922.
10. Ozhinsky E, Vigneron DB, Nelson SJ. Improved spatial coverage for brain 3D PRESS MRSI by automatic placement of outer-volume suppression saturation bands. *J Magn Reson Imaging*. 2011;33:792–802.
11. Osorio JA, Xu D, Cunningham CH, et al. Design of cosine modulated very selective suppression pulses for MR spectroscopic imaging at 3T. *Magn Reson Med*. 2009;61:533–540.
12. Spielman DM, Pauly JM, Macovski A, Glover GH, Enzmann DR. Lipid-suppressed single- and multisection proton spectroscopic imaging of the human brain. *J Magn Reson Imaging*. 1992;2:253–262.
13. Ebel A, Govindaraju V, Maudsley AA. Comparison of inversion recovery preparation schemes for lipid suppression in 1H MRSI of human brain. *Magn Reson Med*. 2003;49:903–908.
14. Young K, Govind V, Sharma K, Studholme C, Maudsley AA, Schuff N. Multivariate statistical mapping of spectroscopic imaging data. *Magn Reson Med*. 2010;63:20–24.
15. Maudsley AA, Domenig C, Sheriff S. Reproducibility of serial whole-brain MR spectroscopic imaging. *NMR Biomed*. 2010;23:251–256.
16. Maudsley AA, Domenig C, Govind V, et al. Mapping of brain metabolite distributions by volumetric proton MR spectroscopic imaging (MRSI). *Magn Reson Med*. 2009;61:548–559.
17. Stagg CJ, Knight S, Talbot K, Jenkinson M, Maudsley AA, Turner MR. Whole-brain magnetic resonance spectroscopic imaging measures are related to disability in ALS. *Neurology*. 2013;80:610–615.
18. Maudsley AA, Domenig C, Ramsay RE, Bowen BC. Application of volumetric MR spectroscopic imaging for localization of neocortical epilepsy. *Epilepsy Res*. 2010;88:127–138.
19. Zhu H, Ouwerkerk R, Barker PB. Dual-band water and lipid suppression for MR spectroscopic imaging at 3 Tesla. *Magn Reson Med*. 2010;63:1486–1492.
20. Zhu H, Edden RA, Ouwerkerk R, Barker PB. High resolution spectroscopic imaging of GABA at 3 Tesla. *Magn Reson Med*. 2011;65:603–609.
21. Esmaeili M, Bathen TF, Rosen BR, Andronesi OC. Three-dimensional MR spectroscopic imaging using adiabatic spin echo and hypergeometric dual-band suppression for metabolic mapping over the entire brain. *Magn Reson Med*. 2017;77:490–497.
22. Maudsley AA, Matson GB, Hugg JW, Weiner MW. Reduced phase encoding in spectroscopic imaging. *Magn Reson Med*. 1994;31:645–651.
23. Hu X, Patel M, Chen W, Ugurbil K. Reduction of truncation artifacts in chemical-shift imaging by extended sampling using variable repetition time. *J Magn Reson B*. 1995;106:292–296.
24. Hugg JW, Maudsley AA, Weiner MW, Matson GB. Comparison of k-space sampling schemes for multidimensional MR spectroscopic imaging. *Magn Reson Med*. 1996;36:469–473.
25. Ebel A, Maudsley AA. Comparison of methods for reduction of lipid contamination for in vivo proton MR spectroscopic imaging of the brain. *Magn Reson Med*. 2001;46:706–712.
26. Metzger G, Sarkar S, Zhang X, Heberlein K, Patel M, Hu X. A hybrid technique for spectroscopic imaging with reduced truncation artifact. *Magn Reson Imaging*. 1999;17:435–443.
27. Adalsteinsson E, Star-Lack J, Meyer CH, Spielman DM. Reduced spatial side lobes in chemical-shift imaging. *Magn Reson Med*. 1999;42:314–323.
28. Haupt CI, Schuff N, Weiner MW, Maudsley AA. Removal of lipid artifacts in 1H spectroscopic imaging by data extrapolation. *Magn Reson Med*. 1996;35:678–687.
29. de Beer R, van den Boogaart A, van Ormondt D, et al. Application of time-domain fitting in the quantification of in vivo 1H spectroscopic imaging data sets. *NMR Biomed*. 1992;5:171–178.
30. Ramirez RR, Kopell BH, Butson CR, Hiner BC, Baillet S. Spectral signal space projection algorithm for frequency domain MEG and EEG denoising, whitening, and source imaging. *NeuroImage*. 2011;56:78–92.
31. Uusitalo MA, Ilmoniemi RJ. Signal-space projection method for separating MEG or EEG into components. *Med Biol Eng Comput*. 1997;35:135–140.
32. Niddam DM, Tsai SY, Lin YR. Statistical mapping of metabolites in the medial wall of the brain: a proton echo planar spectroscopic imaging study. *Hum Brain Mapp*. 2015;36:852–861.
33. Tsai SY, Otazo R, Posse S, et al. Accelerated proton echo planar spectroscopic imaging (PEPSI) using GRAPPA with a 32-channel phased-array coil. *Magn Reson Med*. 2008;59:989–998.

SUPPORTING INFORMATION

Additional supporting information may be found online in the Supporting Information section at the end of the article.

FIGURE S1 (a) MRS phantom without lipid (wo. lip) containing NAA, tCr, Cho, Mi, and Glu; (b) a representative spectrum in the center of wo. lip phantom indicated by the red box in (a); (c) MRS phantom in a container filled with liquid lard as analogue of lipids (w. lip); (d) a representative spectrum in the center of w. lip phantom indicated by red box in (c); (e) a representative spectrum in the region of the w. lip phantom indicated by the yellow box in (c). We can observe some lipid signals in the center region of w. lip phantom (d)

FIGURE S2 Spectra of noSSP, SSP1, SSP3, SSP6 and SSP10 from MRS phantom with lipid (w lip). The locations of voxels are indicated by the red box in the image. From the voxel at lipid region (left top), lipid signals can be significantly suppressed using SSP but there are residue baselines ranging from 1.6 to 2.8 ppm even using SSP10. the residue baseline distortions can also be found on the spectra in non-lipid region of the phantom. The residue baseline distorts the NAA peaks on the spectra in the center of phantom (left bottom). In this voxel, the concentrations of NAA are 22.1 mM, 21.9 mM, 21.9 mM, 20.8 mM, 19.0 mM for noSSP, SSP1, SSP3, SSP6, SSP10

FIGURE S3 Mean, SD and CRLB of the lipid signals within the inner and peripheral ROIs. The results of NOVS and OVS are indicated as dashed and dotted lines, respectively. The results of SSP using 1 to 10 components and PG+SSP using components from 1 to 10 are shown with the error bars from the standard deviation between subjects. The reported lipid signals were quantified by the LCModel (lip13a+lip13b). The fitted lipid signals and their spatial variations decreased to a consistent level for PG+SSP and SSP using more than 4 components. For the lipid signals, the rejection criteria of CRLB are CRLB = 999%

FIGURE S4 Spectra of NOVS, SSP5, SSP10 and lipid signals by SSP5 and SSP10. The spectra are from voxels (a) at the central brain and (b) the peripheral brain near the cranial lipid region from a subject. The locations of voxels are indicated by the red dot on the lipid projection images

How to cite this article: Tsai S-Y, Lin Y-R, Lin H-Y, Lin F-H. Reduction of lipid contamination in MR spectroscopy imaging using signal space projection. *Magn Reson Med*. 2018;00:1–13. https://doi.org/10.1002/mrm.27496